Experimental Neurology 312 (2019) 33–42

Contents lists available at ScienceDirect

Experimental Neurology

journal homepage: www.elsevier.com/locate/yexnr

Research paper

Genetic ablation of Gpr37l1 delays tumor occurrence in *Ptch1*$^{+/-}$ mouse models of medulloblastoma

Chiara Di Pietro[1], Gina La Sala[1], Rafaele Matteoni, Daniela Marazziti[*,2], Glauco P. Tocchini-Valentini[2]

Institute of Cell Biology and Neurobiology, Italian National Research Council (CNR), I-00015, Monterotondo Scalo, Rome, Italy

ARTICLE INFO

Keywords:
Cerebellum
Gpr37l1
Ptch1
Medulloblastoma
Wnt3

ABSTRACT

The G-protein coupled receptor 37-like 1 (Gpr37l1) is specifically expressed in most astrocytic glial cells, including cerebellar Bergmann astrocytes and interacts with patched 1 (Ptch1), a co-receptor of the sonic hedgehog (Shh)-smoothened (Smo) signaling complex. *Gpr37l1* null mutant mice exhibit precocious post-natal cerebellar development, with altered Shh-Smo mitogenic cascade and premature down-regulation of granule cell precursor (GCP) proliferation. *Gpr37l1* expression is downregulated in medulloblastoma (MB) and upregulated in glioma and glioblastoma tumors.

Shh-associated MBs originate postnatally, from dysregulated hyperproliferation of GCPs in developing cerebellum's external granular layer (EGL), as shown in heterozygous *Ptch1*$^{+/-}$ knock-out mouse strains that model human MB occurrence and progression.

This study investigates cerebellar MB phenotypes in newly produced *Gpr37l1, Ptch1* double mutant mice. Natural history analysis shows that *Gpr37l1* genetic ablation, in *Ptch1*$^{+/-}$ model animals, results in marked deferment of post-natal tumor occurrence and decreased incidence of more aggressive tumor types. It is also associated with the delayed and diminished presence of more severe types of hyperplastic lesions in *Ptch1*$^{+/-}$ mice. Consistently, during early post-natal development *Gpr37l1*$^{-/-}$;*Ptch1*$^{+/-}$ pups exhibit reduction in cerebellar GCP proliferation and EGL thickness and a precocious, sustained expression of wingless-type MMTV integration site member 3 (Wnt3), a specific inhibitor of Shh-induced neuronal mitogenesis, in comparison with *Ptch1*$^{+/-}$ heterozygous single mutants. These findings highlight the specific involvement of Gpr37l1 in modulating postnatal cerebellar Shh-Ptch1-Smo mitogenic signaling in both normal and pathological conditions. The novel *Gpr37l1*$^{-/-}$;*Ptch1*$^{+/-}$ mouse models may thus be instrumental in the detailed characterization of the initial phases of Shh-associated MB insurgence and development.

1. Introduction

The vertebrate G-protein coupled receptor 37 and G-protein coupled receptor 37-like 1 (GPR37 and GPR37L1) proteins are homologous to 7-transmembrane spanning, G-protein coupled receptors for endothelin and bombesin peptides (Marazziti et al., 1997; Marazziti et al., 1998; Valdenaire et al., 1998). Secreted cyto-protective protein and peptides have been suggested as possibly interacting with both putative receptors (Liu et al., 2017; Meyer et al., 2013; Smith, 2015). Murine Gpr37l1 can also have neuroprotective effects during ischemia (Jolly et al., 2017), while its absence may result in increased seizure susceptibility (Giddens et al., 2017).

The mammalian *Gpr37l1* gene is extensively expressed in most astrocytic glial cells, including cerebellar Bergmann glia (BG) astrocytes (Chaboub et al., 2016; Jolly et al., 2017; Koirala and Corfas, 2010; Marazziti et al., 2013). In BG astrocytes, the murine Gpr37l1 protein has been shown to interact with patched 1 (Ptch1), a membrane component of the sonic hedgehog (Shh) receptor complex (Marazziti et al., 2013). *Gpr37l1* null mutant mice exhibit a precocious post-natal cerebellar development, as a consequence of altered Shh-smoothened (Smo) mitogenic signaling, with premature down-regulation of neuronal granule cell precursor (GCP) proliferation and concomitant

* *Corresponding author at: Institute of Cell Biology and Neurobiology, Italian National Research Council (CNR), Via E. Ramarini 32, I-00015, Monterotondo Scalo, Rome, Italy.
E-mail address: daniela.marazziti@cnr.it (D. Marazziti).
[1] Co-first authors.
[2] Co-last authors.

https://doi.org/10.1016/j.expneurol.2018.11.004
Received 17 August 2018; Received in revised form 6 November 2018; Accepted 15 November 2018
Available online 16 November 2018
0014-4886/

development and maturation of BG astrocytes and Purkinje neurons (Di Pietro et al., 2016; Marazziti et al., 2013). Genome and transcriptome analyses have reported somatic mutations and transcriptional upregulation of the Gpr37l1 gene in various types of human glioma and glioblastoma (Ceccarelli et al., 2016; Johnson et al., 2014) and its downregulation in human and mouse medulloblastoma (MB) samples (Lee et al., 2003; Whittier et al., 2013).

Highly malignant, cerebellar MB is one of the most frequently diagnosed pediatric brain tumor (Packer, 1999). Distinct MB types are identified according to specific gene expression profiling subgroups: Shh and wingless-type MMTV integration site (Wnt) subgroups, as well as non-Shh, non-Wnt subgroups 3 and 4 (Northcott et al., 2012). Murine strains that are heterozygous for loss-of-function *Ptch1* alleles have been established as in vivo models of Shh-associated MB tumorigenesis (Goodrich et al., 1997; Hahn et al., 1998). Homozygous *Ptch1* null mutants are embryonic lethal with widespread defects in the nervous system and other tissues, while *Ptch1*$^{+/-}$ mice can survive to adulthood, with about 15–30% of all individuals developing MB before 1 year of age (Goodrich et al., 1997; Hahn et al., 1998; Pazzaglia et al., 2006). Moreover, it has been reported that Shh signaling is constitutively activated in *Ptch1*$^{+/-}$ MB tissues (Goodrich et al., 1997; Oliver et al., 2005; Wetmore et al., 2000).

In the murine *Ptch1*$^{+/-}$ models, numerous hyperplastic lesions arise as a consequence of the up-regulated Shh-Smo mitogenic cascade and neuronal GCP hyper-proliferation in the external granular layer (EGL), during post-natal cerebellar development. From ca. 4 weeks onwards, a limited number of lesions undergo malignant transformation to MB initiation and progression (Corcoran et al., 2008; Farioli-Vecchioli et al., 2012; Oliver et al., 2005), which can only occur in the presence of ad hoc local cytological and histological conditions, including specific microenvironmental alterations of intercellular signaling and interactions among Shh-producing Purkinje neurons, proliferating GCPs and maturing BG astrocytes (Martirosian et al., 2016).

This study focused on the possible contribution of Gpr37l1-mediated signaling to MB oncogenesis in *Ptch1*$^{+/-}$ murine models, given Gpr37l1's specific interaction with Ptch1 in BG astrocytes and the premature down-regulation of postnatal GCP proliferation upon genetic inactivation of the Gpr37l1 gene (Marazziti et al., 2013). The experimental results demonstrated that the genetic ablation of Gpr37l1 was associated with both a marked delay in tumor occurrence (to > 10 weeks of age) in *Ptch1*$^{+/-}$ murine models of Shh-subgroup MB and evident prevalence of classic/desmoplastic tumor types (Ayrault et al., 2009; Louis et al., 2016; Pickles et al., 2018). Lack of Gpr37l1, also resulted in the deferred and diminished presence of the more extended, severe types of hyperplastic cerebellar lesions frequently found in non-tumor bearing *Ptch1*$^{+/-}$ animals. Consistently, at the early stages of post-natal cerebellar development *Gpr37l1*$^{-/-}$;*Ptch1*$^{+/-}$ pups exhibited a pronounced reduction in GCP proliferation and EGL thickness, as well as the precocious, striking overexpression of wingless-type MMTV Integration Site Family, Member 3 (Wnt3), a specific inhibitor of Shh-induced neuronal mitogenesis (Anne et al., 2013), with an associated reduction in the level of glioma-associated oncogene family zinc finger 2 (Gli2) protein, the main transcriptional activator that mediates Shh signaling (Wechsler-Reya and Scott, 1999).

Taken together, these findings highlight the specific involvement of Gpr37l1 in modulating postnatal cerebellar Shh-Ptch1-Smo mitogenic signaling in both normal and pathological conditions, with particularly critical effects at the initial stages of dysregulated GCP hyper-proliferation and MB oncogenic transformation and progression in *Ptch1*$^{+/-}$ models. The novel *Gpr37l1*$^{-/-}$;*Ptch1*$^{+/-}$ mouse line could then be instrumental to further analyze and characterize at the molecular and cytological level the very early phases of Shh-associated MB initiation and development, with parallel assessment of potential applications in the study of novel clinical and pharmacological approaches.

2. Materials and methods

2.1. Animal strains and housing

The murine *B6.129-Ptch1*^{tm1Zim} (*Ptch1*$^{+/-}$) heterozygous strain (Hahn et al., 1998) was provided by the INFRAFRONTIER-European Mouse Mutant Archive (EMMA) Core Structure, Consiglio Nazionale delle Ricerche, Monterotondo (EMMA strain ID: EM:00159; https://www.infrafrontier.eu/search?keyword=00159#). A local breeding colony was established, following one backcross to C57BL/6J wild-type background. *Ptch1*$^{+/-}$ males were then crossed with *B6;129-Gpr37l1*$^{tm1.2Gtva}$ (*Gpr37l1*$^{+/-}$) heterozygous females (Marazziti et al., 2013) to produce double heterozygous mice (*Gpr37l1*$^{+/-}$;*Ptch1*$^{+/-}$). The other described *Gpr37l1* and *Ptch1* allelic combinations were obtained according to standard breeding schemes. Genotypes were determined by PCR from the DNA extracted from tail biopsies, as previously described (Hahn et al., 1998; Marazziti et al., 2013). A natural history study was carried out to examine tumor onset, upon daily observation of each scored mouse during the first 12 months of life. All animals were euthanized when they were moribund, or when extracranial tumors were evident, and MB analyzed. The presence of hydrocephalus was evaluated upon necropsy. The sacrifice date was scored as the death date. The natural history study showed a total tumor incidence of 18/65, 34/159, and 15/80 born mice by 12 months of age, while 3, 5 and 1 animals died with no tumor development (*Gpr37l1*$^{+/+}$;*Ptch1*$^{+/-}$, *Gpr37l1*$^{+/-}$;*Ptch1*$^{+/-}$, *Gpr37l1*$^{-/-}$;*Ptch1*$^{+/-}$ genotypes, respectively).

MB's pathological and histological features were assessed as described (Louis et al., 2016; Pickles et al., 2018). Standard histological preparations (hematoxylin and eosin) were applied to evaluate distinctive cytological characteristics, including large cell/anaplastic tumor types. Histopathological MB variants were identified and scored according to the corresponding World Health Organization (WHO) classification (Table 1; Louis et al., 2016; Pickles et al., 2018).

Other mice were sacrificed at selected ages (P10, P16, P25, 10 weeks and 1 year) for histopathology analysis of normal cerebellar tissue and/or to detect precocious MB occurrence and progression into advanced tumors.

After weaning, mice were housed by litter of the same sex, 3 to 5 per cage and maintained in a temperature-controlled room at 21 ± 2 °C, on a 12-h light-dark cycle (lights on at 07:00 a.m.), with food and water available ad libitum. All animals were born and bred in a specific pathogen-free facility and were subjected to experimental protocols, as reviewed and approved by the Animal Health Directorate of the Italian Ministry of Health, according to the ethical and safety rules and guidelines for the use of animals in biomedical research provided by European Union's directives (n. 86/609/EEC and 2010/63/EU) and relevant Italian and international laws and regulations.

Table 1
Characterization of MB in *Gpr37l1*$^{+/+}$;*Ptch1*$^{+/-}$ and *Gpr37l1* −/−;*Ptch1* +/− mice.

	Gpr37l1$^{+/+}$;*Ptch1*$^{+/-}$		*Gpr37l1*$^{-/-}$;*Ptch1*$^{+/-}$	
Tumor type (Ayrault et al., 2009)	*No. of mice*	*%*	*No. of mice*	*%*
Non invasive	12	66.6	11	73.3
Invasive	6	33.3	4	26.6
Hydrocephalus	9	50	5	33
Histological type (Pickles et al., 2018)				
Classic/desmoplastic	12	66.6	15	100
Extensive nodularity/large cell/anaplastic	6	33.3	0	0

2.2. Antibodies used for immunofluorescence labeling

Brain lipid binding protein (Blbp; 1:100, Millipore, Temecula, CA, USA); calbindin 1 (Calb1/CalbD-28 K; 1:200, clone CB-955, Sigma-Aldrich, St. Louis, MO, USA); cyclin-dependent kinase inhibitor 1B (Cdkn1B/p27Kip1; 1:200, clone 57; BD Biosciences); glial fibrillary acidic protein (Gfap; 1:50, clone 4A11, BD Pharmingen, Allschwil, Switzerland); glial high affinity glutamate transporter (glutamate aspartate transporter, Glast; 1:100, Novus Biologicals, Littleton, CO, USA); Gpr37l1 (1:100, clone 7-4A1 Mab Technologies, Stone Mountain, GA, USA); antigen identified by monoclonal antibody Ki-67 (Ki67/Mki67 antigen; 1:100, ThermoFisher, Waltham, MA, USA); phosphohistone H3 complex (PH3; 1:200, Millipore); vesicular glutamate transporter 1 (Vglut1; 1:1000, Synaptic System, Goettingen, Germany); vesicular glutamate transporter 2 (Vglut2; 1:100, clone 8G9.2, Millipore); vimentin (1:100, Sigma-Aldrich), wingless-type MMTV Integration Site Family, Member 3 (Wnt3; 1:200, D-9, Santa Cruz Biotechnology, Santa Cruz, CA, USA).

2.3. Histology, immunofluorescence and quantitative analysis

Entire brains were removed, fixated and sectioned from P10 pups (before the occurrence of any MB symptom) or from mice with MB (according to the natural history study). De-paraffined sagittal sections were stained with hematoxylin and eosin (Sigma-Aldrich) or processed for immunofluorescence labeling and 4′,6-diamidino-2-phenylindole (DAPI; Thermo Fisher Scientific, Waltham, MA, USA) staining, according to standard protocols with antigen retrieval. Fluorescence and bright-field micrographs were acquired with a motorized LMD7000 microscope or with TCS SP5 laser scanning confocal microscope (Leica Microsystems). For quantification of cerebellar layer thickness of P10 pups, 3 images (at identical locations in the cerebellar vermis, between lobules V and VI) from 3 different animals of each genotype group were analyzed with the ImageJ analysis software (National Institute of Mental Health, National Institutes of Health, Bethesda, MD). Histopathological MB variants were identified and scored as indicated above (Table 1; Louis et al., 2016; Pickles et al., 2018).

2.4. Quantitative PCR analysis

Adult *Gpr37l1*$^{+/+}$;*Ptch1*$^{+/-}$ mice with or without MB were used to extract total cerebellar RNA from tumorous or normal tissue areas. First-strand cDNA was then synthesized using the Superscript II synthesis kit (Invitrogen Inc., Carlsbad, CA, USA) according to manufacturer's protocol. RT-quantitative PCR (qPCR) reactions were performed using the ABI PRISM 7000 Sequence Detection System, with TaqMan Gene Expression Master Mix (Applied Biosystems, Foster City, CA, USA). Predesigned real-time PCR assay reagents were purchased (Life Technologies, Carlsbad, CA, USA) for the mouse *Gpr37l1* (Mm00661872_m1) and glyceraldehyde 3-phosphate dehydrogenase (*Gapdh*; 4352932E) genes. All of the experiments were run in triplicate, and the results were normalized to *Gapdh* expression. Results were quantified by the comparative threshold method (Livak and Schmittgen, 2001) and delta-delta cycle threshold (Ct) values were expressed relative to the average value of normal adult cerebellum.

2.5. Pre-neoplastic lesion analysis

Healthy mice were sacrificed at selected ages (P25, 10 weeks, and 1 year) for histopathological detection and analysis of hyperplastic cerebellar lesions and their pre-tumorigenic progression. De-paraffined sagittal sections were processed as indicated above, cerebellar lesions were identified along the entire mediolateral axis and their area was measured with the ImageJ software, upon staining with hematoxylin and eosin (Sigma-Aldrich) or by Ki67 immunolabeling and DAPI staining. Ki67-labeled cells in cerebellar lesions were quantified with the ImageJ analysis software. The number of positive cells was counted in 3 non-adjacent sections from 2 to 5 animals of each genotype and age group and plotted as the mean percentage of positive cells over the total number of cells. All measurements were performed with the observer blind to the identity of the slides.

2.6. Cell proliferation and differentiation analysis

Sectioned brains from MB-bearing mice or from P10 or P16 pups were immunolabeled with antibodies specific for PH3 (1:200, Millipore) or p27Kip1 (1:200, BD Biosciences) and DAPI staining according to standard protocols with antigen retrieval.

PH3-labeled cells in EGL of P10 pups, in preneoplastic region of P16 pups or in tumorous areas of MB-bearing mice were quantified with the ImageJ analysis software. Sections of similar size in similar regions were chosen and analyzed. The average count of positive cells was obtained from 3 non-adjacent sections from each animal ($n = 3$) and plotted as the mean number of positive cells/area. All measurements were performed with the observer blind to the identity of the slides.

2.7. Western blot analysis

Protein extracts were prepared from whole cerebella of P10 pups or adult animals ($n = 3$). Tissue samples were homogenized in lysis buffer (120 mM NaCl, 20 mM HEPES, 5 mM EDTA, 10% glycerol, 1% Triton X-100, Roche complete protease inhibitors), cleared by centrifugation and the protein content of the supernatant was quantified by Biorad DC assay (Bio-Rad Laboratories, Hercules, CA, USA). Protein samples (50 μg) were separated by SDS-PAGE and analyzed by Western blot, according to standard protocols. Protein antigens were labeled with primary antibodies specific for: Shh (1:400, Santa Cruz Biotechnology), Ptch1 (1:1000, clone 413,220, R&D Systems, Minneapolis, MN, USA), Gpr37l1 (1:1000, clone 7-4A1 Mab Technologies), Glast (EAAT1; 1:200, Santa Cruz Biotechnology), glioma-associated oncogene family zinc finger 2 (Gli2; 1:500; Abcam), Wnt3 (1:1000, Santa Cruz Biotechnology), α-tubulin (1:1000, clone DM 1A, Sigma-Aldrich). Horseradish peroxidase-conjugated secondary antibodies, specific for mouse or rat (Amersham Biosciences-GE Healthcare, Piscataway, NJ, USA) immunoglobulins were used, following producer's instructions. The blotted membranes were then processed for chemiluminescence detection with an ECL kit (Amersham) and imaging and quantification of immunoreactive bands (Chemidoc XRS+ imager and Image Lab software, Bio-Rad).

The intensity of each band was normalized to the intensity of the corresponding α-tubulin band. The average values of each experimental group were expressed in arbitrary units, as a ratio to the mean values obtained from the *Gpr37l1* wild-type control group at P10.

2.8. Statistical analysis

Unless otherwise noted, all data are expressed as mean ± SEM and were analyzed using Prism 5 (GraphPad Software, La Jolla, CA, USA). The level of significance was set at $P < 0.05$.

3. Results

3.1. Absence of Gpr37l1 markedly delays MB occurrence in Ptch1$^{+/-}$ mice

The possible influence of *Gpr37l1* on MB incidence and progression was studied, upon production and application of novel *Gpr37l1, Ptch1* murine double mutant models (Hahn et al., 1998; Marazziti et al., 2013). MB incidence in heterozygous *Ptch1*$^{+/-}$ mouse lines varies according to their genetic background, with a greater tendency observed upon backcrossing to C57BL/6 wild-type background (Mille et al., 2014). The *Ptch1*$^{+/-}$ strain (Hanh et al. 1998; > 10 backcrossing generations to C57BL/6) was crossed to mixed (ca. 75% C57BL/6, 25%

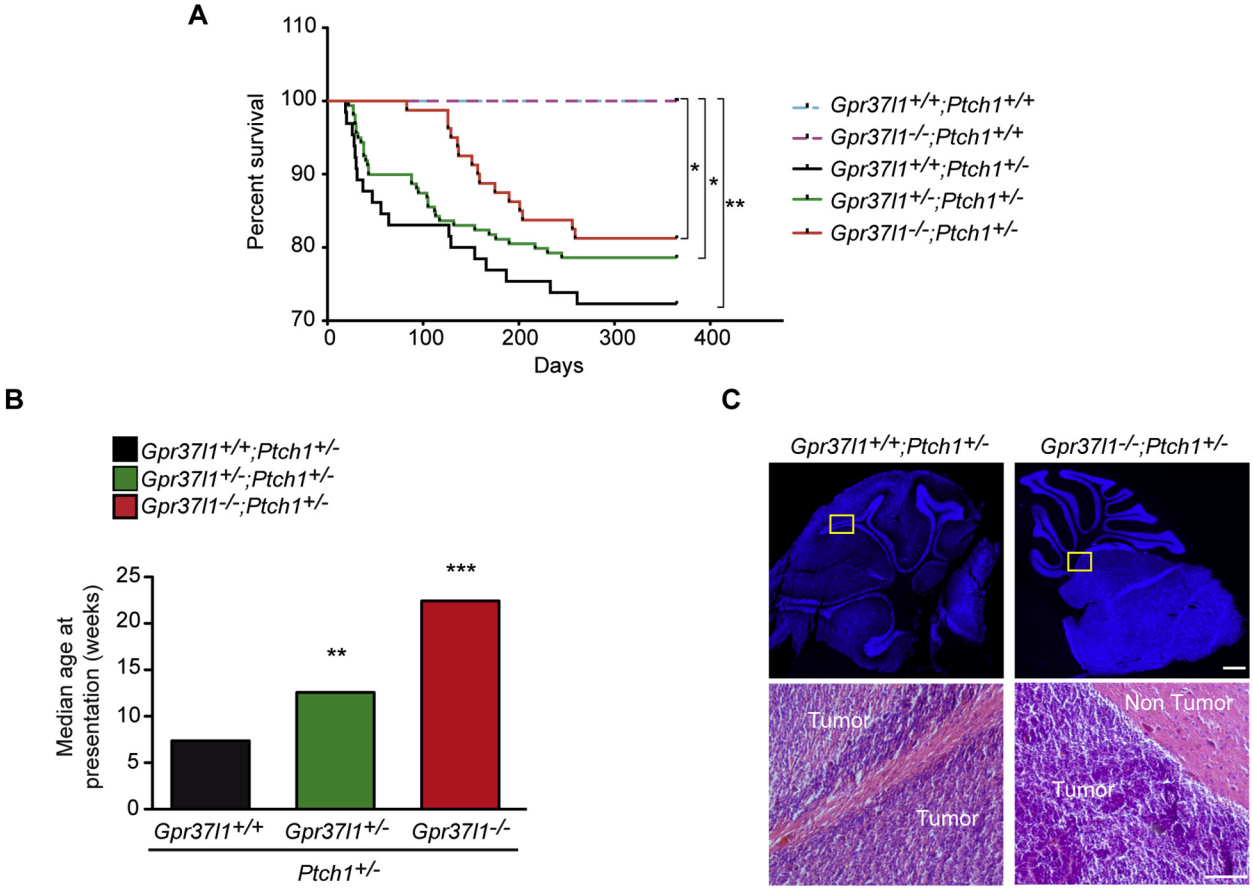

Fig. 1. MB survival curves, age distribution and tumor morphology in *Gpr37l1*$^{+/+}$;*Ptch1*$^{+/-}$, *Gpr37l1*$^{+/-}$;*Ptch1*$^{+/-}$ and *Gpr37l1*$^{-/-}$;*Ptch1*$^{+/-}$ mice. (**A**) Kaplan-Meier survival curves, comparing mice expressing two (*Gpr37l1*$^{+/+}$;*Ptch1*$^{+/-}$ $n = 65$), one (*Gpr37l1*$^{+/-}$;*Ptch1*$^{+/-}$ $n = 159$), or no (*Gpr37l1*$^{-/-}$;*Ptch1*$^{+/-}$ $n = 80$) *Gpr37l1* wild-type alleles, followed over the first 12 months of age. The occurrence or absence of MB was checked in each scored mouse. Control groups included *Gpr37l1*$^{+/+}$;*Ptch1*$^{+/+}$ ($n = 25$) and *Gpr37l1*$^{-/-}$;*Ptch1*$^{+/+}$ (n = 25) mice. Log-rank (Mantel-Cox) tests were performed. Statistical significance was determined using GraphPad Prism software (version 5.0), with *P*-values < .05 as significance threshold (**$P < 0.005$, *Gpr37l1*$^{+/+}$;*Ptch1*$^{+/+}$ vs. *Gpr37l1*$^{+/+}$;*Ptch1*$^{+/-}$; *$P < 0.05$, *Gpr37l1*$^{-/-}$;*Ptch1*$^{+/+}$ vs. *Gpr37l1*$^{-/-}$;*Ptch1*$^{+/-}$; *Gpr37l1*$^{+/+}$;*Ptch1*$^{+/+}$ vs. *Gpr37l1*$^{+/-}$;*Ptch1*$^{+/-}$). (**B**) Median age of MB symptom onset in *Gpr37l1*$^{+/+}$;*Ptch1*$^{+/-}$, *Gpr37l1*$^{+/-}$;*Ptch1*$^{+/-}$ or *Gpr37l1*$^{-/-}$;*Ptch1*$^{+/-}$ mice. Statistical significance was determined using GraphPad Prism software (version 5.0). ***$P < 0.0005$, *Gpr37l1*$^{+/+}$;*Ptch1*$^{+/-}$ vs. *Gpr37l1*$^{-/-}$;*Ptch1*$^{+/-}$; ** $P < 0.006$, *Gpr37l1*$^{+/+}$;*Ptch1*$^{+/-}$ vs. *Gpr37l1*$^{+/-}$;*Ptch1*$^{+/-}$, Wilcoxon rank test. (**C**) Upper panels: representative DAPI staining (blue) of cerebellar tumor sagittal sections from adult *Gpr37l1*$^{+/+}$;*Ptch1*$^{+/-}$ (left) or *Gpr37l1*$^{-/-}$;*Ptch1*$^{+/-}$ (right) mice. Lower panels: higher magnification, representative micrographs of cerebellar hematoxylin-eosin staining, corresponding to upper panel's boxed areas (yellow line) at boundaries between normal tissues and tumors, from adult *Gpr37l1*$^{+/+}$;*Ptch1*$^{+/-}$ (left) or *Gpr37l1*$^{-/-}$;*Ptch1*$^{+/-}$ (right) mice. Scale bars: 500 μm (upper panels), 100 μm (lower panels).

129 wild-type background) *Gpr37l1* heterozygous null mutants (Hahn et al., 1998; Marazziti et al., 2013). *Gpr37l1*$^{+/-}$;*Ptch1*$^{+/-}$, *Gpr37l1*$^{+/+}$;*Ptch1*$^{+/-}$ and *Gpr37l1*$^{-/-}$;*Ptch1*$^{+/-}$ colonies, as well as the other resulting genotype groups, were derived and maintained by subsequent sibling intercross and assessed for the incidence of lethality caused by MB during the first year of age. As expected, survival analysis indicated that wild-type Ptch1 mice (*Gpr37l1*$^{+/+}$;*Ptch1*$^{+/+}$ and *Gpr37l1*$^{-/-}$;*Ptch1*$^{+/+}$) did not develop MB (Fig. 1A). Gpr37l1-expressing, *Ptch1* heterozygous mutants developed lethal MB with an incidence of 27.7% (*Gpr37l1*$^{+/+}$;*Ptch1*$^{+/-}$) or 21.4% (*Gpr37l1*$^{+/-}$;*Ptch1*$^{+/-}$), similar to the original *Ptch1*$^{+/-}$ single-mutant animals (Fig. 1A) (Goodrich et al., 1997; Hahn et al., 1998; Pazzaglia et al., 2006). Remarkably, lack of functional Gpr37l1 in *Gpr37l1*$^{-/-}$;*Ptch1*$^{+/-}$ mice resulted in lower incidence (18.7%) and significantly delayed development of MB (Fig. 1A). The temporal analysis of tumor presentation showed that the median age of onset in the Gpr37l1$^{-/-}$;Ptch1$^{+/-}$ group was 22.43 weeks, with an highly significant difference compared to 7.35 and 12.57 weeks in the *Gpr37l1* wildtype and *Gpr37l1*$^{+/-}$ heterozygous group, respectively (Fig. 1B). Consistently, MBs were present before 10 weeks of age in the majority of *Gpr37l1*$^{+/+}$;*Ptch1*$^{+/-}$ and *Gpr37l1*$^{+/-}$;*Ptch1*$^{+/-}$ mice (11 animals with tumor before 10 weeks of age over a total of 18 animals with tumor, 11/18 = 61.0% and 16/34 = 47.1%, respectively), while tumors were detected between 20 and 30 weeks of age in most *Gpr37l1*$^{-/-}$;*Ptch1*$^{+/-}$ animals (7/15 = 46.6%) (Fig. 1A). The overall analysis of the relative survival curves showed a consistent, albeit not significant, trend (Fig. 1A). In most cases, the tumors displaced and compressed the normal cerebellar architecture (Fig. 1C). Comparison of cerebellar samples from adult, tumor-bearing *Gpr37l1*$^{+/+}$;*Ptch1*$^{+/-}$ and *Gpr37l1*$^{-/-}$;*Ptch1*$^{+/-}$ mice (Table 1) showed a lower incidence of MB-induced hydrocephalus, in the absence of Gpr37l1. This was accompanied by a higher incidence of noninvasive tumors, which were confined to the periphery of the cerebellum and a lower proportion of tumors that invaded normal areas of the cerebellum (Table 1). (Wetmore et al., 2000; Ayrault et al., 2009). Histopathological analysis (Table 1; Fig. 1C) also revealed a strong prevalence of classic/desmoplastic MB and the lack of highly proliferating, large cells/anaplastic tumors in *Gpr37l1*$^{-/-}$;*Ptch1*$^{+/-}$ samples (Louis et al., 2016; Pickles et al., 2018).

Marked immunolabeling of reactive gliosis markers Gfap and vimentin (Kumanishi et al., 1985; Zamanian et al., 2012) was observed in tumor areas, from *Gpr37l1*$^{+/+}$;*Ptch1*$^{+/-}$ and *Gpr37l1*$^{-/-}$;*Ptch1*$^{+/-}$ mice (Fig. 2A, B), with minimal or absent expression of glial high

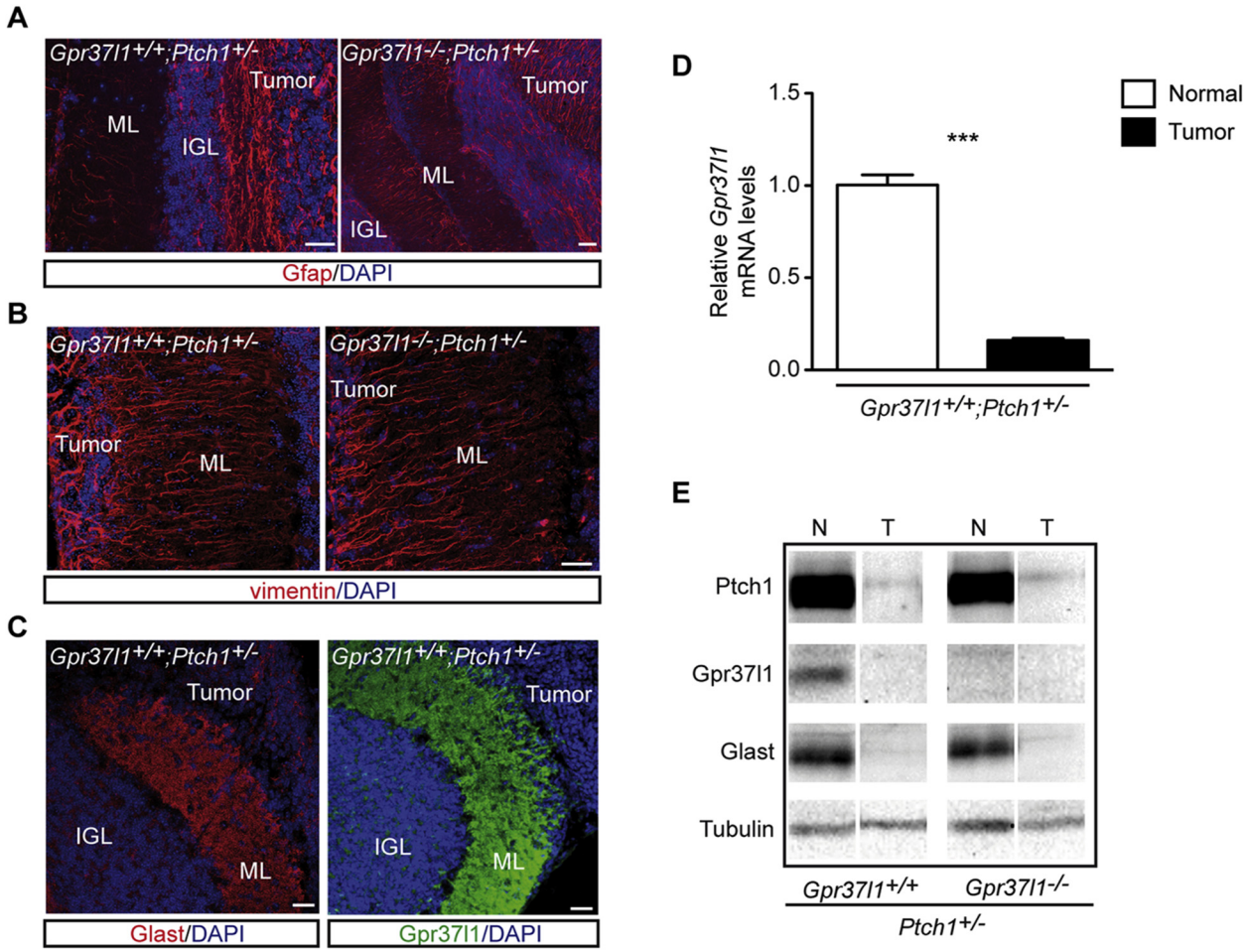

Fig. 2. Glial and Shh pathway marker expression in adult cerebella of *Gpr37l1*$^{+/+}$;*Ptch1*$^{+/-}$ and *Gpr37l1*$^{-/-}$;*Ptch1*$^{+/-}$ mice with or without MB. (**A**, **B**) Representative images of glial fibrillary acidic protein (Gfap; red, A) or vimentin (red, B) immunofluorescence labeling and nuclear DAPI staining (blue) in MB and adjacent areas of adult *Gpr37l1*$^{+/+}$;*Ptch1*$^{+/-}$ or *Gpr37l1*$^{-/-}$;*Ptch1*$^{+/-}$ cerebella. (**C**) Representative images of glial high affinity glutamate transporter (Glast; red, left panel) or Gpr37l1 (green, right panel) immunofluorescence labeling and nuclear DAPI staining (blue), in MB and adjacent areas of adult *Gpr37l1*$^{+/+}$;*Ptch1*$^{+/-}$ cerebella. Scale bars: 50 μm (**A**, **B**), 25 μm (**C**). ML, molecular layer; IGL, internal granular layer. (**D**) Quantitative PCR analysis of *Gpr37l1* expression in normal or tumorous tissue from adult *Gpr37l1*$^{+/+}$;*Ptch1*$^{+/-}$ cerebella. Data are shown as mean ± s.e.m. (n = 3 mice per group), ***P < 0.0001, normal tissue vs. tumorous tissue, unpaired t-test. (**E**) Representative Western blot analysis of cerebellar samples from *Gpr37l1*$^{+/+}$;*Ptch1*$^{+/-}$ and *Gpr37l1*$^{-/-}$;*Ptch1*$^{+/-}$ mice. Adult animals of both genotypes with (T) or without (N) MB were used to prepare cerebellar protein extracts.

affinity glutamate transporter (Glast), a specific Bergmann glia marker (Fig. 2C, E). Immunolabeling and quantitative PCR assays of adult *Gpr37l1*$^{+/+}$;*Ptch1*$^{+/-}$ MB samples also showed drastically reduced levels of *Gpr37l1* mRNA and protein (Fig. 2C, D). Both *Gpr37l1*$^{+/+}$;*Ptch1*$^{+/-}$ and *Gpr37l1*$^{-/-}$;*Ptch1*$^{+/-}$ tumorous tissues showed similar, very reduced expression of the Shh co-receptor, Ptch1, in comparison to normal tissues, as previously reported for single-mutant, *Ptch1*$^{+/-}$ animals (Fig. 2E) (Oliver et al., 2005).

3.2. Absence of Gpr37l1 delays and reduces occurrence of hyperplastic lesions in *Ptch1*$^{+/-}$ mice

Sample groups (n = 8–12) of healthy, non MB-bearing *Gpr37l1*$^{+/+}$;*Ptch1*$^{+/-}$ and *Gpr37l1*$^{-/-}$;*Ptch1*$^{+/-}$ animals at P25, 10 weeks and 1 year of age were separately sacrificed to study and compare occurrence and progression of hyperplastic lesions in the two genotype groups. Lesions were identified by histological staining and immunolabeling of Ki67-positive cells (Matsuo et al., 2013; Tamayo-Orrego et al., 2016) and scored according to their area classification (Fig. 3A). Lack of Gpr37l1 caused the maximal incidence of lesions to be delayed to ca. 10 weeks and drastically reduced their occurrence at 1 year (Fig. 3B). *Gpr37l1*$^{-/-}$;*Ptch1*$^{+/-}$ animals also showed a later (ca. 10 weeks) prevalence of hyperplastic lesions of the more extended types (Fig. 3C; Fig. S1B), with a concomitant, marked increase in the percentage of Ki67-positive cells, in comparison to *Gpr37l1*$^{+/+}$;*Ptch1*$^{+/-}$ mice. Furthermore, the ablation of Gpr37l1 resulted in the absence of large lesions (> 1 mm^2) at 1 year of age (Fig. 3C, D; Fig. S1B).

3.3. Precocious down-regulation of postnatal GCP proliferation in *Gpr37l1*$^{-/-}$;*Ptch1*$^{+/-}$ pups

Cerebellar samples from P10 *Gpr37l1*$^{+/+}$;*Ptch1*$^{+/-}$ (n = 13) and *Gpr37l1*$^{-/-}$;*Ptch1*$^{+/-}$ (n = 16) littermates were analyzed to compare cell proliferation and layering, at a developmental stage when cerebellar development is still ongoing, but preneoplastic lesions are not yet occurring (Mille et al., 2014).

Several specific markers were labeled by immunofluorescence to evaluate neuronal and glial cell proliferation and maturation (Fig. 4) (Marazziti et al., 2013). *Gpr37l1*$^{-/-}$;*Ptch1*$^{+/-}$ pups exhibited a reduced number of granule neurons in EGL and increased BG maturation and Purkinje cell differentiation, in comparison with *Gpr37l1*$^{+/+}$;*Ptch1*$^{+/-}$ P10 pups (Fig. 4, A-D'). Labeling of the proliferating cell nuclear antigen Ki67 (Ki67; Fig. 4, D-D') and the post-mitotic nuclear marker, p27Kip1 (P27; Fig. 4, *E*-E') also showed a lower density of

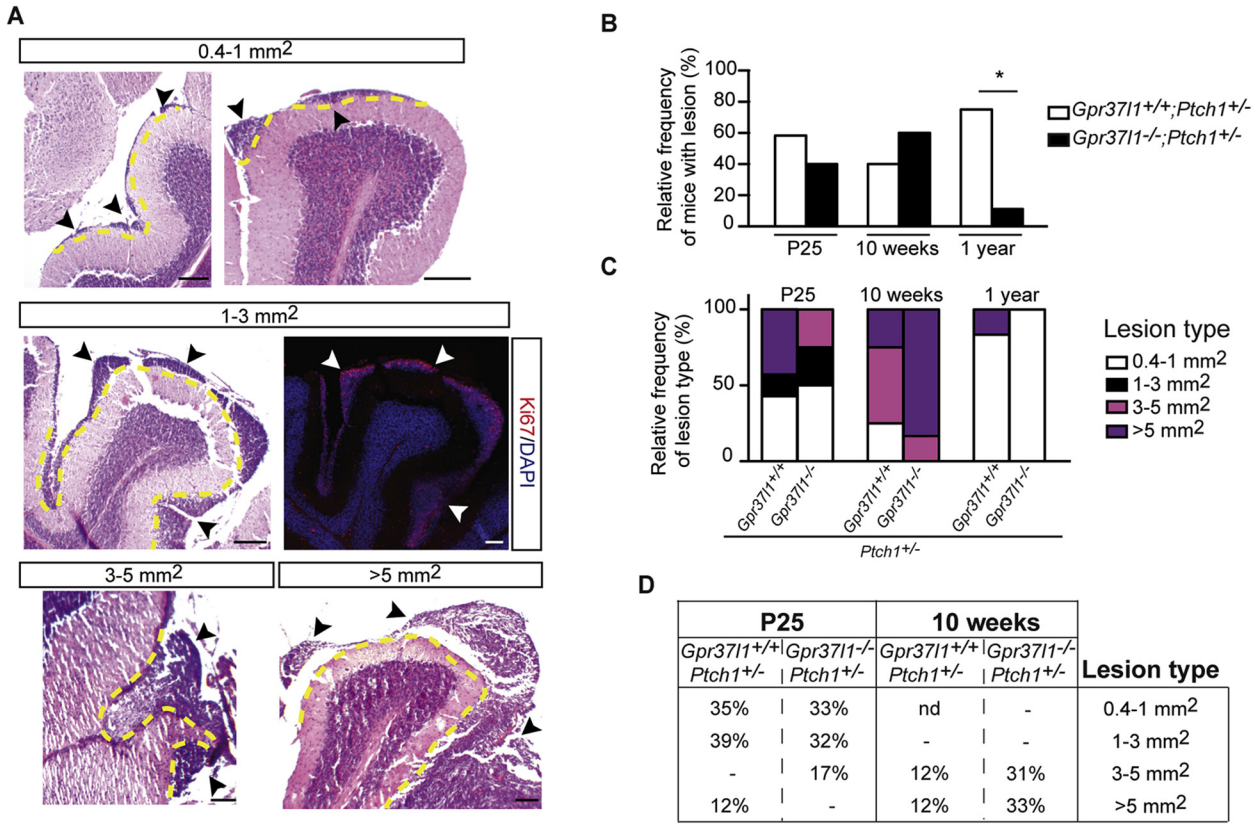

D

P25		10 weeks		
Gpr37l1$^{+/+}$ *Ptch1*$^{+/-}$	*Gpr37l1*$^{-/-}$ *Ptch1*$^{+/-}$	*Gpr37l1*$^{+/+}$ *Ptch1*$^{+/-}$	*Gpr37l1*$^{-/-}$ *Ptch1*$^{+/-}$	Lesion type
35%	33%	nd	-	0.4-1 mm^2
39%	32%	-	-	1-3 mm^2
-	17%	12%	31%	3-5 mm^2
12%	-	12%	33%	>5 mm^2

Fig. 3. Lack of Gpr37l1 delays occurrence and progression of hyperplastic cerebellar lesions. (**A**) Representative hematoxylin-eosin staining of sagittal sections of hyperplastic cerebellar lesions of chosen area groups and immunolabeling of Ki67-positive cells (red) in injured tissues (middle right panel; blue: nuclear DAPI staining), in *Gpr37l1*$^{+/+}$*;Ptch1*$^{+/-}$ and *Gpr37l1*$^{-/-}$*;Ptch1*$^{+/-}$ mice at P25, 10 weeks and 1 year of age. Arrowheads and dashed lines (yellow) indicate hyperplastic lesions. Scale bars: 100 μm. (**B**) Relative frequencies of hyperplastic cerebellar lesions in *Gpr37l1*$^{+/+}$*;Ptch1*$^{+/-}$ and *Gpr37l1*$^{-/-}$*;Ptch1*$^{+/-}$ animals at P25 (*Gpr37l1*$^{+/+}$: 12 mice, 7 with lesions; *Gpr37l1*$^{-/-}$: 10 mice, 4 with lesions), 10 weeks (*Gpr37l1*$^{+/+}$: 10 mice, 4 with lesions; *Gpr37l1*$^{-/-}$: 10 mice, 6 with lesions) and 1 year (*Gpr37l1*$^{+/+}$: 8 mice, 6 with lesions; *Gpr37l1*$^{-/-}$: 9 mice, 1 with lesions) of age. *$P < 0.015$, *Gpr37l1*$^{+/+}$*;Ptch1*$^{+/-}$ vs. *Gpr37l1*$^{+/-}$*;Ptch1*$^{+/-}$, Fisher's exact test. (**C**) Relative frequencies of hyperplastic cerebellar lesions (as scored in **B**) according to their area classification, in *Gpr37l1*$^{+/+}$*;Ptch1*$^{+/-}$ and *Gpr37l1*$^{-/-}$*;Ptch1*$^{+/-}$ animals at P25, 10 weeks and 1 year of age. (**D**) Percentage of Ki67-positive cells in cerebellar lesions (as scored in **B**) according to their area classification, in *Gpr37l1*$^{+/+}$*;Ptch1*$^{+/-}$ and *Gpr37l1*$^{-/-}$*;Ptch1*$^{+/-}$ animals at P25 and 10 weeks. (nd: Ki67-positive cells not detected; hyphens indicate the absence of the corresponding lesion type).

proliferating GCPs in outer EGL, as well as of post-mitotic, differentiating neuronal precursors in inner EGL, in all cerebellar lobes of P10 *Gpr37l1*$^{-/-}$*;Ptch1*$^{+/-}$ pups. Measurements of cerebellar layer thickness confirmed the occurrence of significantly thinner EGL and thicker ML, in P10 *Gpr37l1*$^{-/-}$*;Ptch1*$^{+/-}$ pups compared to *Gpr37l1*$^{+/+}$*;Ptch1*$^{+/-}$ littermates (Fig. 4F and Fig. S2A). Control wild type *Ptch1*$^{+/+}$ pups exhibited a smaller EGL thickness (Fig. S2A), as a consequence of the reported, lower level of GCP proliferation (Hahn et al., 1998).

Wnt3, a specific inhibitor of Shh-induced neuronal mitogenesis (Anne et al., 2013), was also found more extensively expressed in the Purkinje layer (PL), ML and EGL in P10 *Gpr37l1*$^{-/-}$*;Ptch1*$^{+/-}$ samples, consistent with a precocious exertion of its inhibitory effects on proliferating GCPs (Fig. 4C-C').

We assessed the level of proliferation in cerebellar tissues at different MB histopathological stages in *Gpr37l1*$^{+/+}$*;Ptch1*$^{+/-}$ and *Gpr37l1*$^{-/-}$*;Ptch1*$^{+/-}$ mice: EGL at P10, preneoplasia at P16 (one of the earliest stage at which preneoplastic lesions can be distinguished), and advanced MB (tumors obtained from mice with terminal illness). Qualitative and quantitative analysis of phospho-histone H3-positive, proliferating cells were carried out with samples of the above tissues, from both *Gpr37l1*$^{+/+}$*;Ptch1*$^{+/-}$ and *Gpr37l1*$^{-/-}$*;Ptch1*$^{+/-}$ animals (Fig. 5). The lack of Gpr37l1 was found to be associated with a marked reduction in the density of proliferating EGL's neuronal precursors, compared to *Gpr37l1* wild-type controls, while no significant variation of proliferating cell density was detected in preneoplastic or advanced MB samples (Fig. 5B). TUNEL assays revealed minimal, comparable proportions of apoptotic cells in all sampled histopathological stages, from both *Gpr37l1*$^{+/+}$*;Ptch1*$^{+/-}$ and *Gpr37l1*$^{-/-}$*;Ptch1*$^{+/-}$ mice (Fig. S2B). No genotype-specific change of post-mitotic, p27Kip1-positive cell density was detected in preneoplastic or advanced tumor samples, with prevalent nuclear or cytoplasm localization (Fig. S3), respectively, as reported (Bhatia et al., 2009).

Western blot and comparative quantitation of cerebellar protein levels in healthy mice (Fig. 5C, D) showed a precocious, > 2-fold overexpression of Wnt3 in *Gpr37l1*$^{-/-}$*;Ptch1*$^{+/-}$ P10 pups and a non significant tendency to its diminished expression in adults of the same genotype, in comparison with *Gpr37l1* wild-type control samples (Fig. 5C, D). The expression of the Gli2 transcription factor was significantly reduced in *Gpr37l1*$^{-/-}$*;Ptch1*$^{+/-}$ P10 pups (Fig. 5C, D), consistent with the results of previous studies on the precocious upregulation of Wnt3-mediated, anti-proliferative signaling (Anne et al., 2013). The Gli2 protein was absent in all analyzed adult samples, as already reported (Fig. 5C, Kimura et al., 2005). Instead, Shh expression was found not significantly varied in both *Gpr37l1*$^{-/-}$*;Ptch1*$^{+/-}$ P10 and adult samples (Fig. 5D).

4. Discussion

The present study has resulted from the production and analysis of

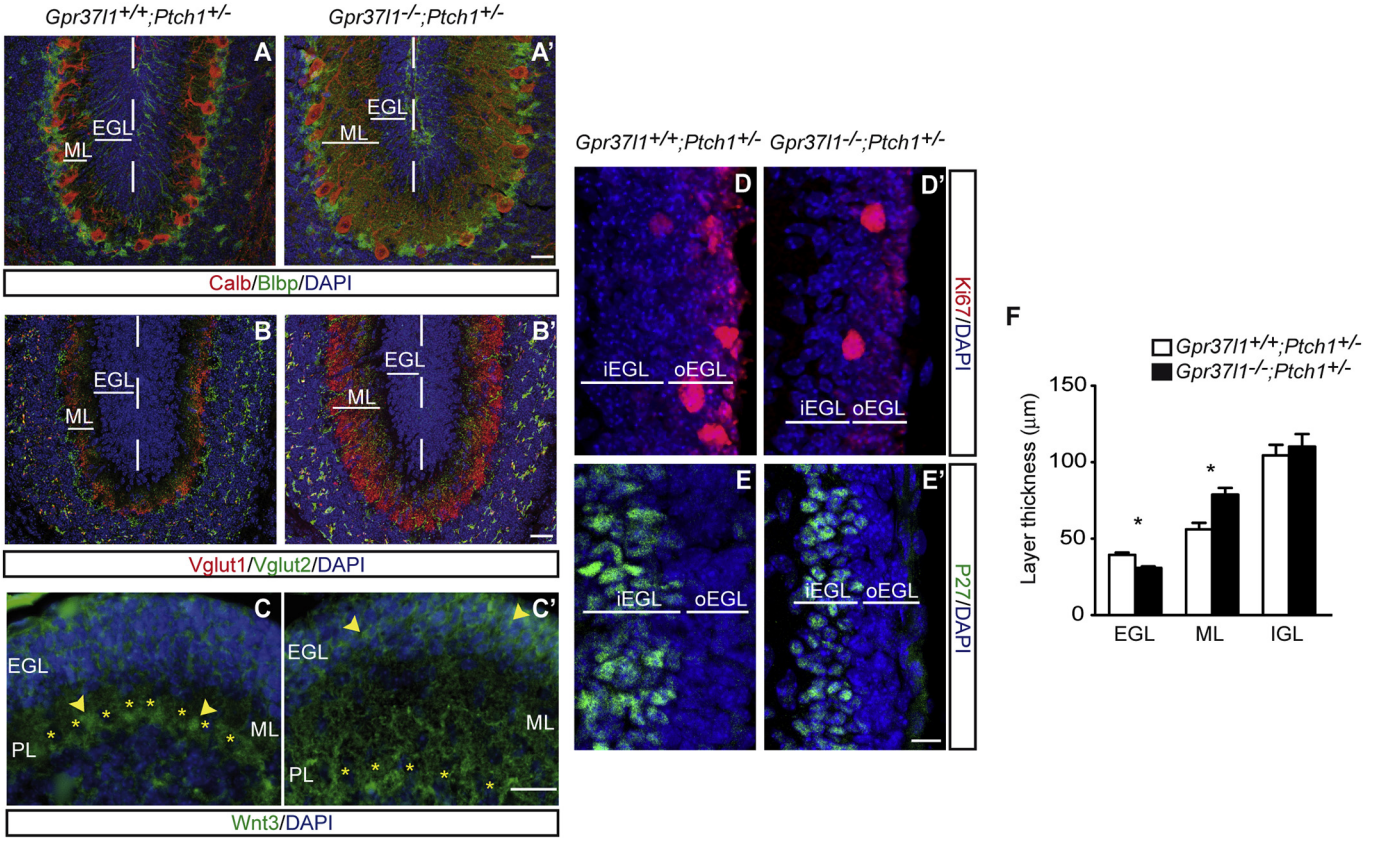

Fig. 4. Cerebellar morphology and cellular proliferation in P10 *Gpr37l1*$^{+/+}$;*Ptch1*$^{+/-}$ and *Gpr37l1*$^{-/-}$;*Ptch1*$^{+/-}$ pups. (**A-A', B-B′**) Representative images of double immunofluorescence labeling with antibodies specific for calbindin 1 (red, Calb) and brain lipid binding protein (green, Blbp), or vesicular glutamate transporter 1 (red, Vglut1) and vesicular glutamate transporter 2 (green, Vglut2), in sagittal cerebellar sections of P10 *Gpr37l1*$^{+/+}$;*Ptch1*$^{+/-}$ (**A**, **B**) or *Gpr37l1*$^{-/-}$;*Ptch1*$^{+/-}$ (A', B′) pups. Nuclei were stained with DAPI (blue). Dashed white lines distinguish EGLs from two adjacent cerebellar lobes. (**C-C′**) Representative images of wingless-type MMTV integration site, member 3 (green, Wnt3) and nuclear DAPI staining (blue), in sagittal cerebellar sections of P10 *Gpr37l1*$^{+/+}$;*Ptch1*$^{+/-}$ (**C**) or *Gpr37l1*$^{-/-}$;*Ptch1*$^{+/-}$ (C′) pups. Yellow arrowheads indicate Wnt3-labeled cells in the Purkinje layer (**C**) or EGL (**C′**). Yellow asterisks mark Purkinje neuron's somata. (**D-E'**). Representative images of Ki67 antigen (red, Ki67, upper panels) or p27Kip1 (green, P27, lower panels) immunofluorescence labeling and nuclear DAPI staining (blue), in sagittal cerebellar sections of P10 *Gpr37l1*$^{+/+}$;*Ptch1*$^{+/-}$ (**D**) or *Gpr37l1*$^{-/-}$;*Ptch1*$^{+/-}$ (**D'**) pups. (**F**) Quantification of EGL, ML and IGL average thickness in P10 *Gpr37l1*$^{+/+}$;*Ptch1*$^{+/-}$ or *Gpr37l1*$^{-/-}$;*Ptch1*$^{+/-}$ pups. Data are shown as mean ± s.e.m.; (n = 3 mice per group). P-values < .05 were used as significance threshold from unpaired two-tailed Student's t-test (*P < 0.05: *Gpr37l1*$^{+/+}$;*Ptch1*$^{+/-}$ vs. *Gpr37l1*$^{-/-}$;*Ptch1*$^{+/-}$). EGL, external granular layer; oEGL, outer portions of EGL; iEGL, inner portions of EGL; ML, molecular layer; PL, Purkinje cell layer. Scale bars: (**A-C′**) 25 µm, (**D-E'**) 10 µm.

the novel *Gpr37l1*$^{-/-}$;*Ptch1*$^{+/-}$ murine model line. It shows that a significant delay in Shh-type MB occurrence and progression occurs in *Ptch1*$^{+/-}$ mice that also lack the functional Gpr37l1 protein. The reported data indicate that the Gpr37l1 putative membrane receptor, a selective marker of cerebellar BG astrocytes (Di Pietro et al., 2016; Marazziti et al., 2013) has a specific role during the initial stages of MB oncogenic transformation and tumorigenesis, as induced by GCP hyperproliferation in *Ptch1*$^{+/-}$ model animals. The absence of Gpr37l1 results, in particular, in the precocious overexpression of Wnt3, with consequent and concurrent inhibitory effects on postnatal granule neuron proliferation.

Previous studies (Di Pietro et al., 2016; Marazziti et al., 2013) have revealed that the mouse Gpr37l1 protein colocalizes and interacts with Ptch1 in BG's membranes and its genetic inactivation alters the timing of GCP proliferation during postnatal cerebellum development, with precocious activation at P3 and down-regulation at P7. BG and Purkinje neurons also undergo anticipated differentiation and maturation and this is accompanied by precocious PC synaptogenesis by climbing and parallel fibers.

Similar alterations of GCP proliferation, BG and Purkinje neurons maturation take place in *Gpr37l1*$^{-/-}$;*Ptch1*$^{+/-}$ pup's cerebella and they counterbalance, at least in part, the concomitant hyper-proliferative effects due to decreased Ptch1 levels. These findings reveal an unanticipated partial dominance of the *Gpr37l1* null mutant phenotype, in the context of *Ptch1* heterozygous loss-of-function mutation, and constitutively activated Shh signaling (Goodrich et al., 1997; Oliver et al., 2005; Wetmore et al., 2000).

Thus, the lack of Gpr37l1 can ultimately reduce the occurrence and severity of *Ptch1*$^{+/-}$-induced hyperproliferating EGL lesions at a critical time window during the first postnatal weeks, with a corresponding delay in the tumorigenic transformation of hyperplastic tissue injuries (at ca. 10 weeks), in agreement with the natural history analysis and other results detailed by the present study.

The experimental data also indicate that mature BG cells, as identified by specific Gpr37l1 and Glast labeling, do not participate to reactive gliosis, which is consequent on MB occurrence and progression. Consistently, Gpr37l1 absence does not significantly affect astrogliosis reaction to tumorous tissue lesions, as well as tumor progression and growth.

It is possible to hypothesize that Shh-Ptch1-Smo mitogenic stimulation at the initial postnatal stages of EGL development may be specifically modulated by Gpr37l1-controlled, functional cross-talk among BG and interacting neuronal cells. Indeed, the genetic ablation of Gpr37l1 results in the increased expression of cerebellar Shh, Smo, Ptch1 and other mitogenic markers at the earliest stages of postnatal murine development (Marazziti et al., 2013).

This study has revealed that the *Gpr37l1* null mutant genotype is also strikingly associated with the precocious, marked overexpression

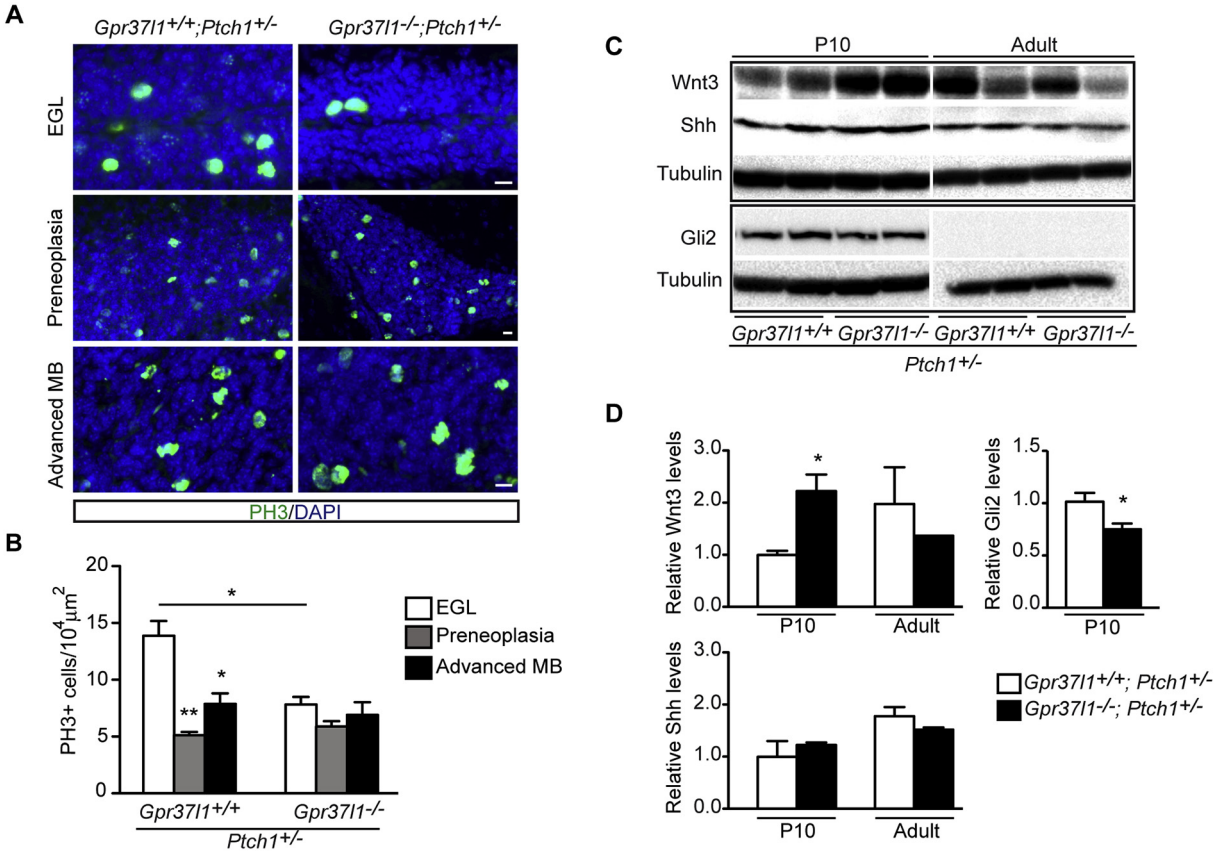

Fig. 5. Cerebellar cell proliferation, Wnt3, Gli2 and Shh protein expression in *Gpr37l1*$^{+/+}$;*Ptch1*$^{+/-}$ and *Gpr37l1*$^{-/-}$;*Ptch1*$^{+/-}$ mice. (**A**) Representative images of phospho-histone H3 complex immunofluorescence labeling (green, PH3) and nuclear DAPI staining (blue) in P10 EGL, P16 preneoplastic and adult advanced MB samples from *Gpr37l1*$^{+/+}$;*Ptch1*$^{+/-}$ or *Gpr37l1*$^{-/-}$;*Ptch1*$^{+/-}$ mice. Scale bars: 10 µm. (**B**) Quantification of PH3-positive cell density in P10 EGL, P16 preneoplastic and adult advanced MB samples from *Gpr37l1*$^{+/+}$;*Ptch1*$^{+/-}$ or *Gpr37l1*$^{-/-}$;*Ptch1*$^{+/-}$ mice. Data are shown as mean ± s.e.m. *P*-values < .05 were used as significance threshold from unpaired two-tailed Student's *t*-test (*$P < 0.05$: *Gpr37l1*$^{+/+}$;*Ptch1*$^{+/-}$ EGL vs. *Gpr37l1*$^{-/-}$;*Ptch1*$^{+/-}$ EGL, *Gpr37l1*$^{+/+}$;*Ptch1*$^{+/-}$ EGL vs. *Gpr37l1*$^{+/+}$;*Ptch1*$^{+/-}$ advanced MB, *Gpr37l1*$^{+/+}$;*Ptch1*$^{+/-}$ preneoplasia vs. *Gpr37l1*$^{+/+}$;*Ptch1*$^{+/-}$ advanced MB. **$P < 0.005$: *Gpr37l1*$^{+/+}$;*Ptch1*$^{+/-}$ EGL vs. *Gpr37l1*$^{+/+}$;*Ptch1*$^{+/-}$ preneoplasia). (**C**) Representative Western blot analysis of cerebellar samples from P10 or adult *Gpr37l1*$^{+/+}$;*Ptch1*$^{+/-}$ and *Gpr37l1*$^{-/-}$;*Ptch1*$^{+/-}$ mice. (**D**) Densitometric quantification of immunostained Wnt3, Shh and Gli2 proteins in whole cerebellar extracts prepared at P10 or adulthood from *Gpr37l1*$^{+/+}$;*Ptch1*$^{+/-}$ or *Gpr37l1*$^{-/-}$;*Ptch1*$^{+/-}$ littermate mice. The average values of each experimental group are expressed in arbitrary units, as a ratio to the mean values obtained from the P10 *Gpr37l1* wild-type control group. Data are shown as mean ± s.e.m. ($n = 3$ mice per group), *$P < 0.05$, *Gpr37l1*$^{+/+}$;*Ptch1*$^{+/-}$ vs. *Gpr37l1*$^{-/-}$;*Ptch1*$^{+/-}$, unpaired *t*-test.

of Wnt3, a specific inhibitor of Shh-induced neuronal mitogenesis, whose production depends on the maturation status of PC (Salinas et al., 1994). The postnatal up-regulation of cerebellar Wnt3 expression critically decreases EGL neuronal precursor's growth, upon inhibition of Shh-mediated signaling through a non-canonical Wnt3-frizzled pathway (Anne et al., 2013; Salinas et al., 1994). Therefore in the *Gpr37l1*$^{-/-}$;*Ptch1*$^{+/-}$ double mutant pups the absence of Gpr37l1 can cause a precocious surge in cerebellar Shh signaling, as well as Wnt3-mediated anti-proliferative effects, including the reported down-regulation of the Gli2 transcription factor (Anne et al., 2013), with consequent, earlier down-regulation of Shh-induced, GCP mitogenesis and of tumorigenesis-susceptible, focal hyperproliferation. It is worth nhoting that the postnatal, cell type-specific ablation of Shh production by developing murine BG astrocytes results in a markedly similar phenotype, including elevated Wnt-mediated signaling and concomitant reduction of the EGL (Cheng et al., 2018). These findings suggest that BG-mediated Shh signaling can specifically regulate Wnt's antagonistic effects on GCP proliferation.

Other reports also indicate that BG astrocytes can process and secrete both Shh and Wnt3 (Farmer et al., 2016; Okuda et al., 2016; Xu et al., 2013) and Gpr37l1 could be involved in regulating their production. For instance, given its direct intracellular interaction with Ptch1 (Marazziti et al., 2013), it could affect Ptch1 trafficking and membrane location and therefore Shh-, Ptch1-dependent autocrine pathways that cross-regulate Shh and Wnt production (Regan et al., 2017). Gpr37l1 might also interact on Wnt-associated, regulating proteins, similar to what already described for the chaperoning effects exerted by the homologous Gpr37 receptor on the Wnt co-receptor, the low-density lipoprotein receptor-related protein 6 (Berger et al., 2017).

In addition, Gpr37l1 could participate in BG's modulation of Shh and Wnt3 production by Purkinje neurons (Ugbode et al., 2017), e.g. by regulating astrocyte's production of cholesterol derivatives or other molecules that are required for post-translational, functional modification of Shh and/or Wnt3 precursors (Cunningham et al., 2015; Ng et al., 2016). Novel detailed studies with ex vivo cerebellar astrocyte and neuronal cultures from wild-type, *Gpr37l1*$^{-/-}$, *Gpr37l1*$^{-/-}$;*Ptch1*$^{+/-}$ pups are being carried out to verify the above hypothesis.

Overall, the newly described *Gpr37l1*$^{-/-}$;*Ptch1*$^{+/-}$ murine line could be suitably applied as an ad hoc model to further investigate the very early phases of Shh-associated MB initiation and progression. Moreover, it could be instrumental to set-up and assess novel genetic or chemical (Ngo et al., 2017) protocols aimed at altering in vivo Gpr37l1's and related protein's functions, for their possible application in novel clinical and pharmacological approaches.

Supplementary data to this article can be found online at https://doi.org/10.1016/j.expneurol.2018.11.004.

Declarations of interest

None.

Acknowledgments

The authors greatly thank K. Havas for helpful discussions and critical reading of the manuscript; G. Bolasco, Microscopy Facility Manager and E. Perlas, Head of Histology Core Facility of EMBL Rome, Epigenetics and Neurobiology Unit for expert assistance with confocal microscopy and histology; G. D'Erasmo and A. Ventrera for excellent technical assistance and A. Ferrara and T. Cuccurullo for secretarial assistance. Supported by Consiglio Nazionale delle Ricerche Progetto d'Interesse Strategico Invecchiamento and European Union Framework Programmes (PHENOSCALE, EUCOMMTools grants).

References

Anne, S.L., Govek, E.E., Ayrault, O., Kim, J.H., Zhu, X., Murphy, D.A., ... Hatten, M.E., 2013. WNT3 inhibits cerebellar granule neuron progenitor proliferation and medulloblastoma formation via MAPK activation. PLoS One 8 (11), e81769. https://doi.org/10.1371/journal.pone.0081769.

Ayrault, O., Zindy, F., Rehg, J., Sherr, C.J., Roussel, M.F., 2009. Two tumor suppressors, p27Kip1 and patched-1, collaborate to prevent medulloblastoma. Mol. Cancer Res. 7 (1), 33–40. https://doi.org/10.1158/1541-7786.MCR-08-0369.

Berger, B.S., Acebron, S.P., Herbst, J., Koch, S., Niehrs, C., 2017. Parkinson's disease-associated receptor GPR37 is an ER chaperone for LRP6. EMBO Rep. 18 (5), 712–725. https://doi.org/10.15252/embr.201643585.

Bhatia, B., Northcott, P.A., Hambardzumyan, D., Govindarajan, B., Brat, D.J., Arbiser, J.L., Holland, E.C., Taylor, M.D., Kenney, A.M., 2009. Tuberous sclerosis complex suppression in cerebellar development and medulloblastoma: separate regulation of mammalian target of rapamycin activity and p27 Kip1 localization. Cancer Res. 69 (18), 7224–7234. https://doi.org/10.1158/0008-5472.CAN-09-1299.

Ceccarelli, M., Barthel, F.P., Malta, T.M., Sabedot, T.S., Salama, S.R., Murray, B.A., ... Verhaak, R.G., 2016. Molecular Profiling reveals Biologically Discrete Subsets and Pathways of Progression in Diffuse Glioma. Cell 164 (3), 550–563 doi:S0092-8674(15)01692-X.

Chaboub, L.S., Manalo, J.M., Lee, H.K., Glasgow, S.M., Chen, F., Kawasaki, Y., ... Deneen, B., 2016. Temporal Profiling of Astrocyte Precursors reveals parallel Roles for Asef during Development and after Injury. J. Neurosci. 36 (47), 11904–11917 (doi:36/47/11904).

Cheng, F.Y., Fleming, J.T., Chiang, C., 2018. Bergmann glial Sonic hedgehog signaling activity is required for proper cerebellar cortical expansion and architecture. Dev. Biol. 440 (2), 152–166. https://doi.org/10.1016/j.ydbio.2018.05.015.

Corcoran, R.B., Bachar Raveh, T., Barakat, M.T., Lee, E.Y., Scott, M.P., 2008. Insulin-like growth factor 2 is required for progression to advanced medulloblastoma in patched1 heterozygous mice. Cancer Res. 68 (21), 8788–8795 (doi:68/21/8788).

Cunningham, D., DeBarber, A.E., Bir, N., Binkley, L., Merkens, L.S., Steiner, R.D., Herman, G.E., 2015. Analysis of hedgehog signaling in cerebellar granule cell precursors in a conditional Nsdhl allele demonstrates an essential role for cholesterol in postnatal CNS development. Hum. Mol. Genet. 24 (10), 2808–2825. https://doi.org/10.1093/hmg/ddv042.

Di Pietro, C., Marazziti, D., La Sala, G., Abbaszadeh, Z., Golini, E., Matteoni, R., Tocchini-Valentini, G.P., 2016. Primary Cilia in the Murine Cerebellum and in Mutant Models of Medulloblastoma. Cell. Mol. Neurobiol. 37 (1), 145–154. https://doi.org/10.1007/s10571-016-0354-3.

Farioli-Vecchioli, S., Cina, I., Ceccarelli, M., Micheli, L., Leonardi, L., Ciotti, M.T., ... Tirone, F., 2012. Tis21 knock-out enhances the frequency of medulloblastoma in Patched1 heterozygous mice by inhibiting the Cxcl3-dependent migration of cerebellar neurons. J. Neurosci. 32 (44), 15547–15564 doi:32/44/15547.

Farmer, W. T., Abrahamsson, T., Chierzi, S., Lui, C., Zaelzer, C., Jones, E. V., … Murai, K. K. (2016). Neurons diversify astrocytes in the adult brain through sonic hedgehog signaling. Science, 351(6275), 849–854. doi:351/6275/849.

Giddens, M.M., Wong, J.C., Schroeder, J.P., Farrow, E.G., Smith, B.M., Owino, S., ... Hall, R.A., 2017. GPR37L1 modulates seizure susceptibility: evidence from mouse studies and analyses of a human GPR37L1 variant. Neurobiol. Dis. 106, 181–190 doi:S0969-9961(17)30157-2.

Goodrich, L.V., Milenkovic, L., Higgins, K.M., Scott, M.P., 1997. Altered neural cell fates and medulloblastoma in mouse patched mutants. Science 277 (5329), 1109–1113. https://doi.org/10.1126/science.277.5329.1109.

Hahn, H., Wojnowski, L., Zimmer, A.M., Hall, J., Miller, G., Zimmer, A., 1998. Rhabdomyosarcomas and radiation hypersensitivity in a mouse model of Gorlin syndrome. Nat. Med. 4 (5), 619–622. https://doi.org/10.1038/nm0598-619.

Johnson, B.E., Mazor, T., Hong, C., Barnes, M., Aihara, K., McLean, C.Y., ... Costello, J.F., 2014. Mutational analysis reveals the origin and therapy-driven evolution of recurrent glioma. Science 343 (6167), 189–193. https://doi.org/10.1126/science.1239947.

Jolly, S., Bazargani, N., Quiroga, A.C., Pringle, N.P., Attwell, D., Richardson, W.D., Li, H., 2017. G protein-coupled receptor 37-like 1 modulates astrocyte glutamate transporters and neuronal NMDA receptors and is neuroprotective in ischemia. Glia 66 (1), 47–61. https://doi.org/10.1002/glia.23198.

Kimura, H., Stephen, D., Joyner, A., Curran, T., 2005. Gli1 is important for medulloblastoma formation in Ptc1 +/− mice. Oncogene 24, 4026–4036. https://doi.org/10.1038/sj.onc.1208567.

Koirala, S., Corfas, G., 2010. Identification of novel glial genes by single-cell transcriptional profiling of Bergmann glial cells from mouse cerebellum. PLoS One 5 (2), e9198. https://doi.org/10.1371/journal.pone.0009198.

Kumanishi, T., Washiyama, K., Watabe, K., Sekiguchi, K., 1985. Glial fibrillary acidic protein in medulloblastomas. Acta Neuropathol. 67 (1–2), 1–5.

Lee, Y., Miller, H.L., Jensen, P., Hernan, R., Connelly, M., Wetmore, C., ... McKinnon, P.J., 2003. A molecular fingerprint for medulloblastoma. Cancer Res. 63 (17), 5428–5437.

Liu, B., Teschemacher, A.G., Kasparov, S., 2017. Astroglia as a cellular target for neuroprotection and treatment of neuro-psychiatric disorders. Glia 65 (8), 1205–1226. https://doi.org/10.1002/glia.23136.

Livak, K.J., Schmittgen, T.D., 2001. Analysis of relative gene expression data using real-time quantitative PCR and the 2(−Delta Delta C(T)) Method. Methods 25 (4), 402–408. https://doi.org/10.1006/meth.2001.1262.

Louis, D.N., Perry, A., Reifenberger, G., Andreas von Deimling, A., Figarella-Branger, D., Cavenee, W.K., Ohgaki, H., Wiestler, O.D., Kleihues, P., Ellison, D.W., 2016. The 2016 World Health Organization Classification of Tumors of the Central nervous System: a summary. Acta Neuropathol. 131 (6), 803–820. https://doi.org/10.1007/s00401-016-1545-1.

Marazziti, D., Golini, E., Gallo, A., Lombardi, M.S., Matteoni, R., Tocchini-Valentini, G.P., 1997. Cloning of GPR37, a gene located on chromosome 7 encoding a putative G-protein-coupled peptide receptor, from a human frontal brain EST library. Genomics 45 (1), 68–77 doi:S0888-7543(97)94900-4.

Marazziti, D., Gallo, A., Golini, E., Matteoni, R., Tocchini-Valentini, G.P., 1998. Molecular cloning and chromosomal localization of the mouse Gpr37 gene encoding an orphan G-protein-coupled peptide receptor expressed in brain and testis. Genomics 53 (3), 315–324 doi:S0888-7543(98)95433-7.

Marazziti, D., Di Pietro, C., Golini, E., Mandillo, S., La Sala, G., Matteoni, R., Tocchini-Valentini, G.P., 2013. Precocious cerebellum development and improved motor functions in mice lacking the astrocyte cilium-, patched 1-associated Gpr37l1 receptor. Proc. Natl. Acad. Sci. U. S. A. 110 (41), 16486–16491. https://doi.org/10.1073/pnas.1314819110.

Martirosian, V., Chen, T.C., Lin, M., Neman, J., 2016. Medulloblastoma initiation and spread: where neurodevelopment, microenvironment and cancer cross pathways. J. Neurosci. Res. 94 (12), 1511–1519. https://doi.org/10.1002/jnr.23917.

Matsuo, S., Takahashi, M., Inoue, K., Tamura, K., Irie, K., Kodama, Y., Nishikawa, A., Yoshida, M., 2013. Thickened area of external granular layer and Ki-67 positive focus are early events of medulloblastoma in Ptch1(+)/(−) mice. Exp. Toxicol. Pathol. 65 (6), 863–873 doi:S0940-2993(12)00149-2.

Meyer, R.C., Giddens, M.M., Schaefer, S.A., Hall, R.A., 2013. GPR37 and GPR37L1 are receptors for the neuroprotective and glioprotective factors prosaptide and prosaposin. Proc. Natl. Acad. Sci. U. S. A. 110 (23), 9529–9534 doi:1219004110.

Mille, F., Tamayo-Orrego, L., Levesque, M., Remke, M., Korshunov, A., Cardin, J., ... Charron, F., 2014. The Shh receptor Boc promotes progression of early medulloblastoma to advanced tumors. Dev. Cell 31 (1), 34–47 doi:S1534-5807(14)00520-6.

Ng, X.W., Teh, C., Korzh, V., Wohland, T., 2016. The Secreted Signaling Protein Wnt3 is Associated with Membrane Domains in Vivo: a SPIM-FCS Study. Biophys. J. 111 (2), 418–429. https://doi.org/10.1016/j.bpj.2016.06.021.

Ngo, T., Ilatovskiy, A.V., Stewart, A.G., Coleman, J.L., McRobb, F.M., Riek, R.P., ... Smith, N.J., 2017. Orphan receptor ligand discovery by pickpocketing pharmacological neighbors. Nat. Chem. Biol. 13 (2), 235–242 (doi:nchembio.2266).

Northcott, P.A., Dubuc, A.M., Pfister, S., Taylor, M.D., 2012. Molecular subgroups of medulloblastoma. Expert. Rev. Neurother. 12 (7), 871–884. https://doi.org/10.1586/ern.12.66.

Okuda, H., Tatsumi, K., Morita-Takemura, S., Nakahara, K., Nochioka, K., Shinjo, T., ... Wanaka, A., 2016. Hedgehog Signaling Modulates the Release of Gliotransmitters from Cultured Cerebellar Astrocytes. Neurochem. Res. 41 (1–2), 278–289. https://doi.org/10.1007/s11064-015-1791-y.

Oliver, T.G., Read, T.A., Kessler, J.D., Mehmeti, A., Wells, J.F., Huynh, T.T., ... Wechsler-Reya, R.J., 2005. Loss of patched and disruption of granule cell development in a pre-neoplastic stage of medulloblastoma. Development 132 (10), 2425–2439 (doi:dev.01793).

Packer, R.J., 1999. Primary Central nervous System Tumors in Children. Curr. Treat. Options Neurol. 1 (5), 395–408.

Pazzaglia, S., Tanori, M., Mancuso, M., Gessi, M., Pasquali, E., Leonardi, S., ... Saran, A., 2006. Two-hit model for progression of medulloblastoma preneoplasia in Patched heterozygous mice. Oncogene 25 (40), 5575–5580 (doi:1209544).

Pickles, J.C., Hawkins, C., Pietsch, T., Jacques, T.S., 2018. CNS embryonal tumours: WHO 2016 and beyond. Neuropathol. Appl. Neurobiol. 44 (2), 151–162. https://doi.org/10.1111/nan.12443.

Regan, J.L., Schumacher, D., Staudte, S., Steffen, A., Haybaeck, J., Keilholz, U., ... Lange, M., 2017. Non-Canonical Hedgehog Signaling is a positive Regulator of the WNT Pathway and is Required for the Survival of Colon Cancer Stem Cells. Cell Rep. 21 (10), 2813–2828. https://doi.org/10.1016/j.celrep.2017.11.025.

Salinas, P.C., Fletcher, C., Copeland, N.G., Jenkins, N.A., Nusse, R., 1994. Maintenance of Wnt-3 expression in Purkinje cells of the mouse cerebellum depends on interactions with granule cells. Development 120 (5), 1277–1286.

Smith, N.J., 2015. Drug Discovery Opportunities at the Endothelin B Receptor-Related Orphan G Protein-coupled Receptors, GPR37 and GPR37L1. Front. Pharmacol. 6, 275. https://doi.org/10.3389/fphar.2015.00275.

Tamayo-Orrego, L., Wu, C.L., Bouchard, N., Khedher, A., Swikert, S.M., Remke, M., Skowron, P., Taylor, M.D., Charron, F., 2016. Evasion of Cell Senescence leads to Medulloblastoma Progression. Cell Rep. 14 (12), 2925–2937. https://doi.org/10.

1016/j.celrep.2016.02.061.
Ugbode, C.I., Smith, I., Whalley, B.J., Hirst, W.D., Rattray, M., 2017. Sonic hedgehog signalling mediates astrocyte crosstalk with neurons to confer neuroprotection. J. Neurochem. 142 (3), 429–443. https://doi.org/10.1111/jnc.14064.
Valdenaire, O., Giller, T., Breu, V., Ardati, A., Schweizer, A., Richards, J.G., 1998. A new family of orphan G protein-coupled receptors predominantly expressed in the brain. FEBS Lett. 424 (3), 193–196 doi:S0014-5793(98)00170-7.
Wechsler-Reya, R.J., Scott, M.P., 1999. Control of neuronal precursor proliferation in the cerebellum by Sonic Hedgehog. Neuron 22 (1), 103–114. https://doi.org/10.1016/S0896-6273(00)80682-0.
Wetmore, C., Eberhart, D.E., Curran, T., 2000. The normal patched allele is expressed in medulloblastomas from mice with heterozygous germ-line mutation of patched. Cancer Res. 60 (8), 2239–2246.
Whittier, K.L., Boese, E.A., Gibson-Corley, K.N., Kirby, P.A., Darbro, B.W., Qian, Q., ... O'Dorisio, M.S., 2013. G-protein coupled receptor expression patterns delineate medulloblastoma subgroups. Acta. Neuropathol. Commun. 1, 66 doi:2051-5960-1-66.
Xu, H., Yang, Y., Tang, X., Zhao, M., Liang, F., Xu, P., ... Fan, X., 2013. Bergmann glia function in granule cell migration during cerebellum development. Mol. Neurobiol. 47 (2), 833–844. https://doi.org/10.1007/s12035-013-8405-y.
Zamanian, J.L., Xu, L., Foo, L.C., Nouri, N., Zhou, L., Giffard, R.G., Barres, B.A., 2012. Genomic analysis of reactive astrogliosis. J. Neurosci. 32 (18), 6391–6410 (doi:32/18/6391).